Indoor Air Quality Implications of Germicidal 222 nm Light

Victoria Barber[1,2*], Matthew B. Goss[1,2], Lesly J. Franco Deloya[3], Lexy N. LeMar[4], Yaowei Li[5], Erik Helstrom[1], Manjula Canagaratna[6], Frank N. Keutsch[5,7,8], Jesse H. Kroll[1,4*]

[1]Department of Civil and Environmental Engineering, Massachusetts Institute of Technology, Cambridge, Massachusetts 02139, United States
[3]Department of Earth, Atmospheric, and Planetary Sciences, Massachusetts Institute of Technology, Cambridge, Massachusetts 02139, United States
[4]Department of Chemical Engineering, Massachusetts Institute of Technology, Cambridge, Massachusetts 02139, United States
[5]John A. Paulson School of Engineering and Applied Sciences, Harvard University, Cambridge, Massachusetts 02138, United States
[6]Center for Aerosol and Cloud Chemistry, Aerodyne Research Incorporated, Billerica, Massachusetts 01821, United States
[7]Department of Chemistry and Chemical Biology, Harvard University, Cambridge, Massachusetts 02138, United States
[8]Department of Earth and Planetary Sciences, Harvard University, Cambridge, Massachusetts 02138, United States
[2]Equal contribution, [*]Corresponding Authors

vbarber@mit.edu,
Massachusetts Institute of Technology
Department of Civil and Environmental Engineering
77 Massachusetts Avenue, 48-330
Cambridge, MA 02139

jhkroll@mit.edu
Massachusetts Institute of Technology
Department of Civil and Environmental Engineering
77 Massachusetts Avenue, 48-331
Cambridge, MA 02139
617-253-2409

Keywords: Ultraviolet Germicidal Irradiation, Indoor Air Quality, Ozone, Photochemistry, Ventilation, Volatile Organic Compounds, Secondary Organic Aerosol

Abstract

A known strategy for mitigating the indoor transmission of airborne pathogens, including the SARS-CoV-2 virus, is irradiation by germicidal UV light (GUV). A particularly promising approach is 222 nm light from KrCl excimer lamps (GUV_{222}); this inactivates airborne pathogens, but is thought to be far less harmful to human skin and eyes than longer-wavelength GUV (e.g., 254 nm). However, the potential for GUV_{222} to affect the composition of indoor air has received little experimental study. Here, we conduct a series of controlled laboratory experiments, carried out in a 150 L Teflon chamber, to examine formation of oxidants and other secondary species by GUV_{222}. We show that GUV_{222} generates ozone (O_3) and hydroxyl radicals (OH), both of which can react with volatile organic compounds to form oxidized volatile organic compounds and secondary organic aerosol particles. Results are consistent with predictions from a simple box model based on known photochemistry. We use this experimentally-validated model to simulate the effect of GUV_{222} irradiation under more realistic indoor air scenarios, spanning a range of light and ventilation conditions. We demonstrate that under some conditions, GUV_{222} irradiation can lead to levels of O_3, OH, and secondary organic products that are substantially elevated relative to normal indoor conditions, especially when ventilation is low and GUV_{222} intensity is high. Thus, GUV_{222} should be used at the lowest intensities possible and in concert with ventilation, decreasing levels of airborne pathogens while mitigating the formation of air pollutants in indoor environments.

Significance Statement

Many respiratory pathogens, including SARS-CoV-2, are spread via airborne transmission. This is particularly problematic in indoor environments, due to limited ventilation. One technique that can reduce levels of indoor airborne pathogens is irradiation by short-wavelength (222 nm) germicidal ultraviolet light (GUV_{222}), which inactivates pathogens while being relatively skin- and eye-safe. However, GUV_{222} implications for indoor air quality have not been investigated in detail. We carry out laboratory studies showing that GUV_{222} forms ozone (an oxidant and respiratory irritant), the hydroxyl radical (a stronger oxidant), and a range of oxidation byproducts, including fine particulate matter. We extrapolate results to more realistic indoor spaces, and show that to minimize negative health impacts, GUV_{222} should be used alongside (rather than instead of) ventilation.

1. Introduction

The COVID-19 pandemic has highlighted the critical need to develop and implement strategies to decrease the transmission of airborne pathogens. Approaches include both source control (isolation, masking), and remediation (ventilation, air cleaning). One approach that has received substantial attention is the use of germicidal ultraviolet (GUV) light, which inactivates airborne pathogens. This approach goes back decades (1), traditionally using 254 nm light from mercury lamps. Since light of this wavelength can cause damage to skin and eyes, care must be taken to minimize occupants' direct exposure to the GUV light (2, 3).

A promising new approach to GUV-based air cleaning is the use of KrCl excimer lamps, which emit at 222 nm (GUV_{222})(4). In contrast to 254 nm GUV, GUV_{222} does not penetrate deeply into biological materials. Therefore, while GUV_{222} is effective at inactivating airborne viruses and bacteria, it is unable to penetrate the outer layer of dead skin cells or the ocular tear layer (5). 222 nm light is hence less likely to reach and damage living human tissues, offering the potential for air disinfection throughout an entire, occupied indoor space.

A risk with GUV_{222}-based air cleaning, as with all types of air cleaning that rely on chemical and/or photolytic processes, is the potential formation of unwanted secondary byproducts (6, 7). A particular concern with GUV_{222} is the formation of ozone (O_3), a harmful air pollutant that acts as a strong oxidant and can lead to respiratory distress when inhaled (8). O_3 is formed by the UV photodissociation of oxygen (R1-2)

$$O_2 + h\nu_{\lambda<242\ nm} \rightarrow O + O \quad \text{(R1)}$$

$$O + O_2 + M \rightarrow O_3 + M \quad \text{(R2)}$$

Since absorption of UV by O_2, and hence O_3 production, is strongest at short wavelengths (9), manufacturers of KrCl lamps have added filters to block wavelengths shorter than 222 nm. But since O_2 absorbs weakly even at 222 nm ($\sigma = 4.09 \times 10^{24}$ cm^2 (9)), all KrCl lamps have the potential to generate ozone, possibly in concentrations higher than is typically found indoors (roughly 5 ppb (10)).

Ozone generated indoors, in addition to posing a direct health hazard, can set off a cascade of chemical reactions that can also affect indoor air quality. Ozone reacts directly with alkenes, present both in the air and on indoor surfaces, forming a range of oxidized volatile organic compounds (OVOCs)(11, 12) and secondary organic aerosol (SOA)(13), which may negatively impact human health (14–17). O_3 chemistry can also lead to the formation of the hydroxyl radical (OH), an even stronger oxidant. This occurs either through reactions with alkenes, which are known to form OH (R3)(11, 18), or through O_3 photolysis (R4-5) (19):

$$\text{Alkene} + O_3 \rightarrow \text{OH} + \text{other products} \quad \text{(R3)}$$

$$O_3 + h\nu_{\lambda<411\ nm} \rightarrow O_2 + O(^1D) \quad \text{(R4)}$$

$$O(^1D) + H_2O \rightarrow 2OH \quad \text{(R5)}$$

Any increased levels of indoor O_3 from GUV_{222} would likely enhance the importance of these reactions, leading to higher levels of indoor OH. This includes O_3 photolysis (R4-5), which is the main source of OH in the troposphere but under normal conditions is negligible in indoor environments, due to the lack of low-wavelength UV. Any OH radicals formed from R3-5 may then oxidize a wide range of organic species and lead to the formation of OVOCs and SOA.

GUV_{222} therefore has the potential to dramatically affect the chemical composition of indoor air, and may lead to the formation of chemical species that are hazardous to human health. However, the extent and nature of this impact remains quite uncertain, even as GUV_{222} is being deployed in indoor spaces (20). Two very recent experimental studies (21, 22) demonstrate O_3 production from GUV_{222}, but these do not examine the overall effects on indoor air quality (including the production of OH, OVOCs, and SOA) by GUV222. To our knowledge the only work that has is a box-modeling study by Peng et al. (23). That work predicted that 222 nm irradiation could lead to elevated levels of O_3 and other secondary species relative to non-illuminated conditions, especially under low-ventilation conditions. To date, such modeling results have yet to be tested experimentally.

Here we describe a series of laboratory experiments aimed at better understanding the effects of 222 nm irradiation on indoor air quality. The goal of this work is to gain process-based insight into how such irradiation affects the chemical composition of the air; we do not examine the effects of GUV_{222} light on pathogens, indoor surfaces, or human health. These experiments, which use a flow-through Teflon chamber coupled to a range of real-time analytical instruments, explore the effects of several parameters relevant to indoor air processes (VOC level, ventilation, 222 nm light intensity, and humidity) on the generation of oxidants and secondary products. Results are then used to validate a simple chemical model of GUV_{222} irradiation of indoor air, which in turn is used to examine the interplay between GUV_{222} and ventilation in controlling the levels of ozone and other chemical species in the indoor environment.

2. Results and Discussion

2.1. Ozone production. The production of ozone by 222 nm light is examined via the irradiation of clean chamber air. Figure 1 shows results from four representative irradiation experiments (average GUV_{222} irradiance = 45 $\mu W/cm^2$), run at different ventilation rates (1.3 to 3.1 air changes per hour (ACH)) and relative humidities (25%-45%). O_3 production is observed to occur immediately when the lights are turned on. O_3 levels increase quickly at first, eventually leveling off to a steady-state value, in which photolytic production is balanced by removal by outflow. The O_3 production rate is measured at 324 ± 18 ppb hr^{-1}), in reasonably good agreement with previous measurements (21) when differences in average GUV_{222} irradiance are considered (see Section S1.1). The steady-state O_3 concentration is independent of relative humidity, and inversely proportional to ventilation rate (Figure S1).

Dashed lines in Figure 1 denote O_3 concentrations predicted from a simple box model, which includes O_2 photolysis (R1-2), O_x-HO_x chemistry, and dilution (model details are given in the Methods and SI). The model accurately predicts measured O_3 levels, indicating that the

processes describing ozone levels (formation from O_3 photolysis at 222 nm, loss by outflow) are well-captured by the simple model.

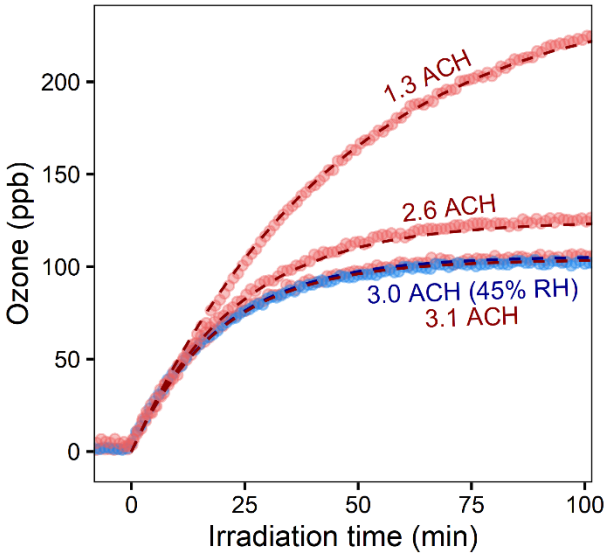

Figure 1: Observed ozone production for clean-chamber irradiation experiments. Measurements agree well with the predictions from the simple box model (dashed lines) across a range of ventilation rates and relative humidities. Measurements shown in red are taken at 25% RH.

2.2. Decay of VOCs upon 222 nm irradiation.

In a second set of experiments (listed in Table S1), VOCs are added to the irradiated chamber after O_3 levels reach steady state. Experiments center on two VOCs: hexanal ($C_6H_{12}O$), a C6 compound that reacts only with OH, and cyclohexene (C_6H_{10}), a C6 compound that reacts with both OH and O_3. VOC decays are shown in Figure 2.

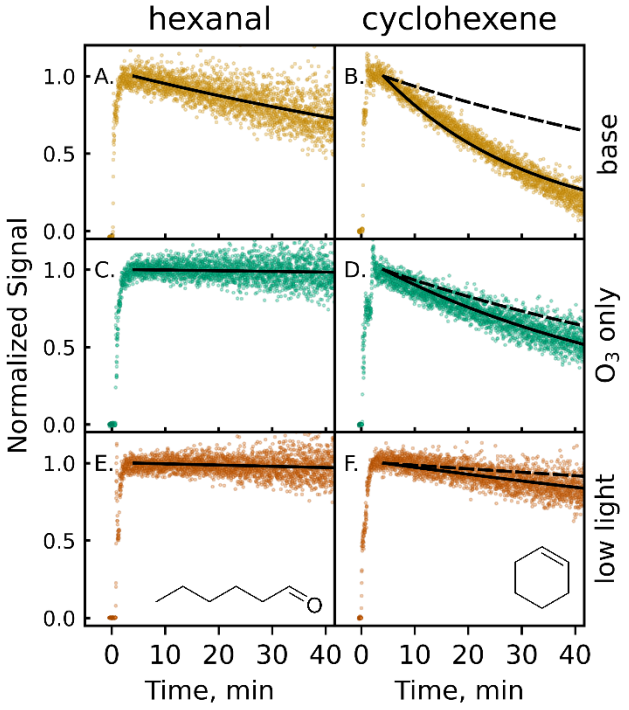

Figure 2: Normalized decays of two VOCs (hexanal and cyclohexene) after introduction to the GUV_{222}-irradiated chamber (see also Figure S2). Time = 0 refers to when the VOC was injected into the chamber. Traces are background- and dilution-corrected, so observed decays are from oxidative loss only. Details of each experimental condition (base, O_3 only, low light) are given in the text and Table S1. Solid black lines denote single-exponential fits to the observed decays; dashed black lines show the expected decay of cyclohexene from reaction with O_3 only (24).

Under "base conditions" (10 ppb VOC precursor, 222 nm light, ~25% RH) (Figure 2AB), the concentrations of both hexanal and cyclohexene decrease after being introduced to the irradiated chamber. Concentrations are corrected for dilution; losses by direct photolysis and uptake to surfaces are expected to be minimal (see Section S1.2). Therefore, decays indicate oxidative loss only. This oxidation cannot be explained by O_3 alone: hexanal does not react with O_3, and while cyclohexene does, its decay is far faster than what can be attributed to the O_3 reaction (dashed line). Indeed, for experiments in which the GUV_{222} light is off and VOCs are exposed to the same levels of O_3 as in the irradiated case (Figure 2CD), the hexanal does not decrease at all, and cyclohexene decays far less than in the irradiation case, at a rate consistent with reaction with O_3 (plus a small contribution from OH generated by the ozonolysis reaction, reaction R3). This observed "excess reactivity" (the difference in observed decays and decays expected from O_3 reaction alone) indicates that GUV_{222} irradiation generates not only O_3 but other oxidants as well.

Additional experiments carried out under a range of reaction conditions provide evidence that these additional oxidants are OH radicals, formed from reactions 3-5. For example, experiments

with the 222 nm light intensity attenuated substantially (~ 9 μW cm^{-2}) exhibit VOC decay rates that are much slower compared to those under base conditions (Figure 2EF). Attenuating light intensity is assumed to decrease steady-state O_3 concentrations proportionally (see methods). However, the observed excess reactivity disproportionately decreases, by approximately an order of magnitude. This is consistent with OH formation, which depends on the photolysis of both O_2 and O_3, as well as (in the case of cyclohexene) the ozonolysis reactions. The dependence of decays on other experimental parameters, such as VOC concentration and relative humidity, are also consistent with OH production from GUV_{222} lights; this is discussed in detail in Section S1.3.

We estimate average OH levels in all experiments, using the excess reactivity and known OH rate constants (25, 26) (see Section S1.4). We also calculate OH levels using our simple box model (see Methods). Measured and modeled average [OH] agree well (Figure 3), providing strong evidence that GUV_{222} produces not only O_3 (R1-2) but also OH (R3-5), and that oxidation by both O_3 and OH can take place upon irradiation with 222 nm light.

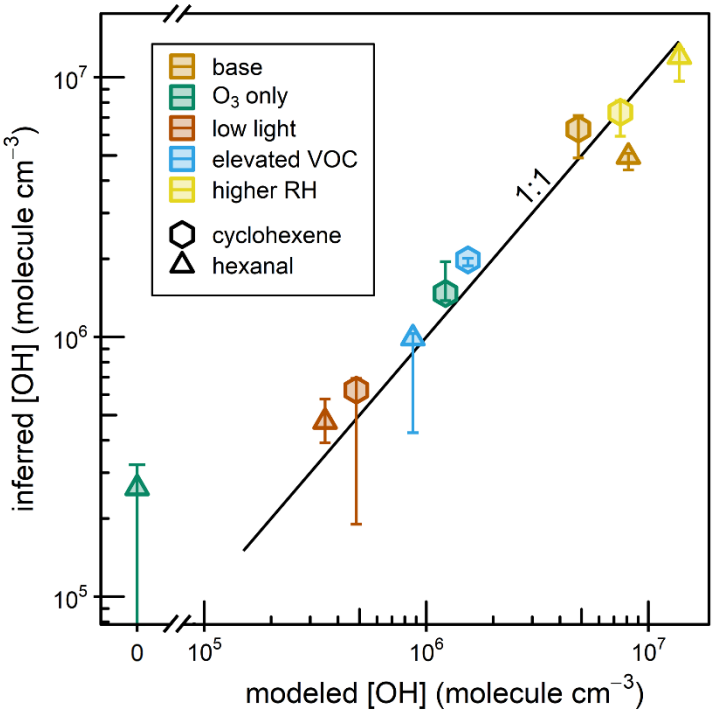

Figure 3: Experimentally-derived average OH concentration vs. average OH concentration predicted by the box model, for all cyclohexene and hexanal experiments (see Section S1.4). Note the break in the x-axis.

2.3 Formation of gas-phase oxidation products. The formation of oxidized gas-phase products is observed in all experiments in which VOC oxidation occurs. Product distributions for three cyclohexene experiments (base conditions, O_3 only, and low light) are shown in Figure 4. Additional product distributions and time-series results (including for the hexanal experiments) are provided in Figures S3 and S4.

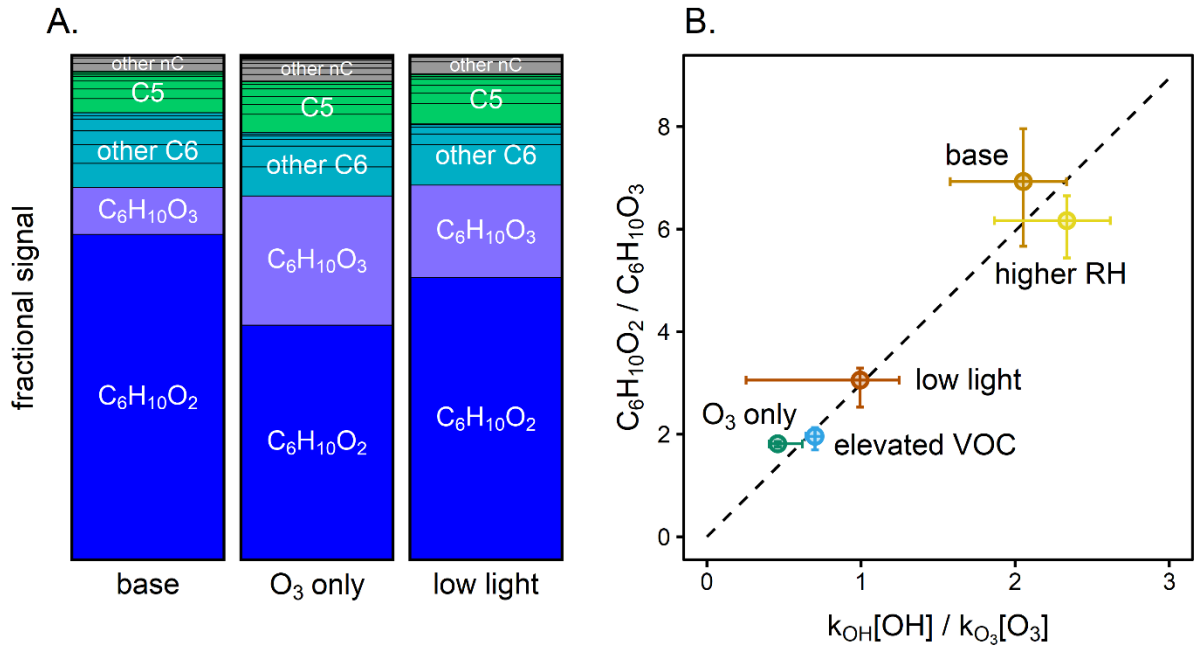

Figure 4: Gas-phase products from cyclohexene experiments. Panel A: Normalized mass spectrometric signal of products formed for the GUV_{222} irradiation (base conditions), O_3-only, and low-light experiments (see Section S1.5 for calculations and Figure S3 for other experimental conditions). Signals are integrated from t = 250 s to 2500 s, normalized to total integrated ion signal and grouped by carbon number (nC). In all cases products are dominated by $C_6H_{10}O_2$ (the major cyclohexene + OH reaction product) and $C_6H_{10}O_3$, (the major cyclohexene + O_3 product). Panel B: The ratio of the $C_6H_{10}O_2$-to-$C_6H_{10}O_3$ signals vs. the ratio of the rates of OH and O_3 oxidation, for all cyclohexene experiments. Concentrations of OH are determined from the fits in Figure 2, while concentrations of O_3 are measured directly. The dashed line is a linear fit to the data; since the two products have differing sensitivities in the instrument, this differs from the 1:1 line. Error bars represent the range of values observed throughout the experiment.

Measured products are dominated by C6 and C5 compounds, as expected given that cyclohexene is a C6 species. The two products with the largest mass spectrometric signals, $C_6H_{10}O_2$ and $C_6H_{10}O_3$, are the major products of the OH and O_3 initiated oxidation of cyclohexene, respectively (27, 28) (see Scheme S1) (Products are detected as the analyte-NH_4^+ adduct, and reported as the analyte formula.) The ratios of the signals from the two products varies among experiments, indicating differences in the relative concentrations of OH and O_3. In Figure 4b, the ratio of the mass spectrometric signals of these two products is shown vs. the relative OH-to-O_3 oxidation rate ratios (calculated from the experimentally-determined values of [OH] and [O_3]) for each cyclohexene experiment. A strong correlation (R^2 = 0.98) is found between the two ratios, providing further support for OH-initiated oxidation, and more generally for OH radical

production from irradiation by 222 nm light. The products formed in the 222 nm irradiation of hexanal are also broadly consistent with OH-initiated oxidation (see Scheme S2) (29).

2.4 Secondary organic aerosol formation. In all experiments, dry ammonium sulfate seed particles are added to the chamber, providing surface area onto which low-volatility species may condense, and enabling the assessment of potential SOA formation. SOA formation is observed in a number of experiments (Table S1 and Figure S5). SOA formation is generally modest for most hexanal and cyclohexene experiments, likely due to the relatively small size (C6) and low concentrations (10 ppb) of those species. Higher concentrations of SOA are observed for experiments with high initial concentrations (100 ppb) of hexanal or cyclohexane, and for those using limonene ($C_{10}H_{16}$, a monoterpene commonly found in fragrances and cleaning products). In fact, the GUV_{222} irradiation of 100 ppb limonene (a level that can be found in indoor environments immediately after cleaning events (30, 31)) results in exceedingly high SOA loadings, on the order of 400 ± 80 μg m^{-3}. Additionally, the formation of new particles is observed upon 222 nm irradiation under some conditions (Section S1.6 and Figure S6). This occurs even when no VOCs are added, and so may result from the oxidation of trace organic species on the chamber walls. Whether this is a general feature of the irradiation of organics on indoor surfaces is unclear from the present experiments, but it does suggest that 222 nm irradiation may induce new particle formation in some environments.

2.5 Extrapolation to indoor environments

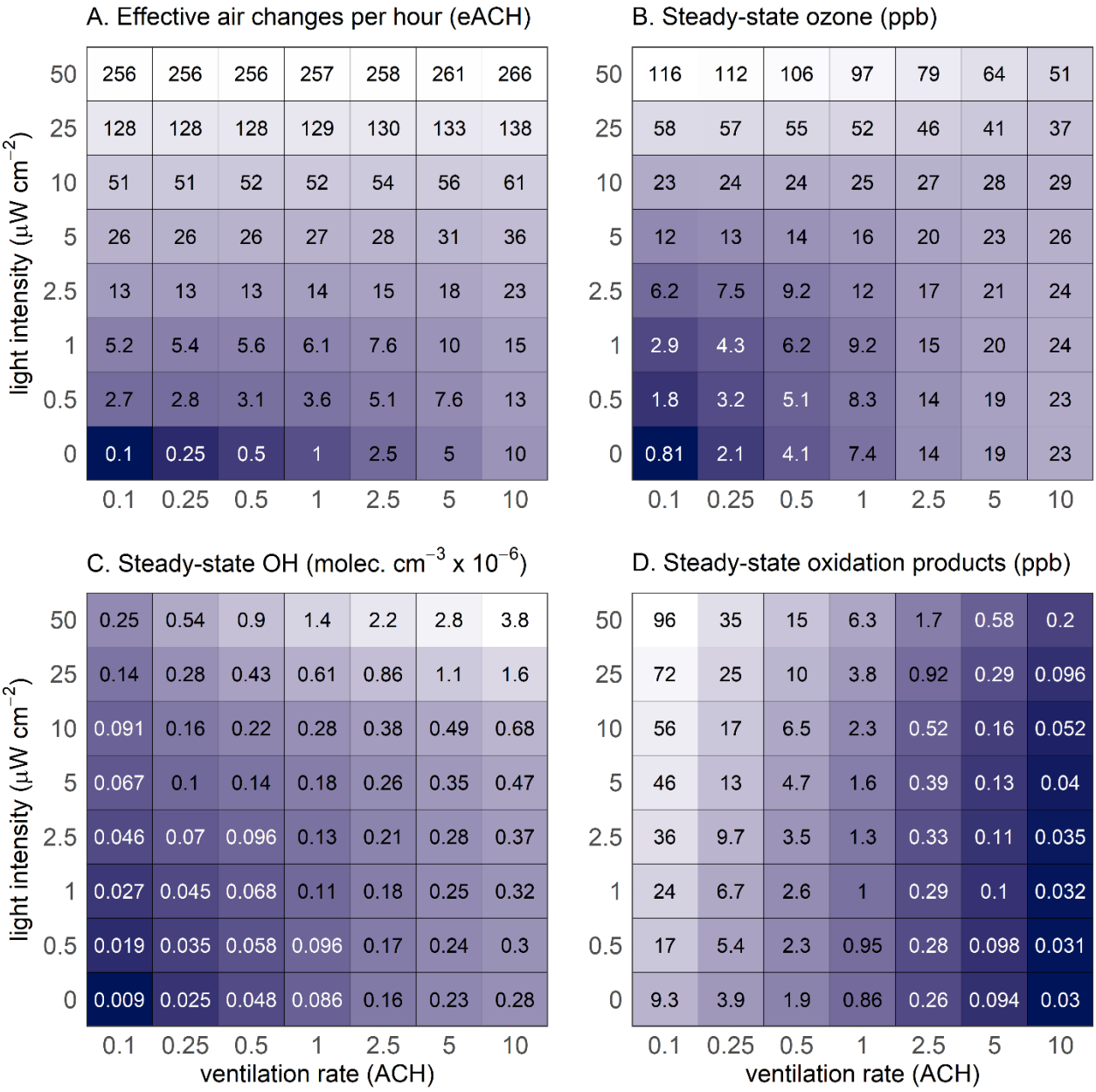

Figure 5: Effects of ventilation and GUV_{222} irradiation on modeled GUV efficacy and indoor air quality (see also Figures S7 and S8). Panel A: effective air changes per hour (eACH) for indoor pathogens, based on the previously reported inactivation rate of SARS-CoV-2 at 222 nm (32) (Section S2.1). Panels B-D: steady-state concentrations of (B) O_3, (C) OH, and (D) organic oxidation products, respectively, as predicted by the photochemical box model. Panel D calculations assume unit yields, and do not account for VOC production from surfaces, so likely represent lower limits. Lighter colors represent larger values; note that the logarithmic color scaling is different for each panel.

The above laboratory experiments demonstrate that GUV_{222} irradiation forms ozone, OH, and a range of oxidation products; measured ozone and inferred OH agree broadly with predictions by a photochemical box model. However real-world indoor environments are more complex than our simple laboratory system, as they involve a large number of organic compounds, depositional loss of ozone and other species, infiltration of outdoor pollutants, and a wide range of possible ventilation rates. Here we extend our photochemical model to a more realistic indoor air scenario, with the goal of understanding how GUV_{222} may impact indoor air quality under a range of ventilation and irradiation conditions. The expanded model is described in detail in the Methods and in SI. Briefly, reactive VOCs are not simulated individually but rather as "lumped" species, defined by their OH and O_3 reactivities, which are chosen based on previous measurements of indoor air (33, 34). The model is run at 298 K, 1 atm, and 30% RH. We also include a background concentration of O_3 in the ventilation air (40 ppb, consistent with typical outdoor O_3 concentrations), a 25% loss of O_3 to the ventilation system, and an O_3 deposition constant of 3 hr^{-1} (10, 35).

The range of light intensities chosen covers US and international guidelines on 222 nm exposure limits (ranging from 0.8 to 16 $\mu W/cm^2$ over 8 hours (36, 37)) as well as the values in previous studies used for pathogen deactivation (average intensities of 0.09 to 14.4 $\mu W/cm^2$ at 1.7 m above the ground from Eadie et al. (38) and 3.5 $\mu W/cm^2$ from Peng et al. (23)). Ventilation rates span a range of typical indoor values, and include the minimum American Society of Heating, Refrigerating and Air-Conditioning Engineers (ASHRAE) recommendations for homes (0.35 ACH), offices (~2-3 ACH), and health care settings (10 ACH)(39).

Key model results are provided in Figure 5. Figure 5A shows the effective air change rate (eACH) across a wide range of 222 nm light intensities and ventilation rates; even modest irradiation levels lead to substantial increases in eACH (see also Figure S7A). Figures 5B, C, and D show the steady-state indoor concentrations of O_3, OH, and total oxidation products (assuming unit yield), respectively.

Steady-state ozone levels (Figure 5B) are higher with 222 nm irradiation than without. Sources of O_3 include photochemistry (R1-2) and infiltration of outdoor air, while sinks include deposition, ventilation, and chemical reaction (rates and contributions of individual processes are given in Figures S7B-E). With low irradiation, O_3 levels are governed mainly by infiltration of outdoor air, and O_3 increases are modest. Under the highest irradiation levels (>25 $\mu W/cm^2$), and especially under low ventilation rates (<1 ACH), indoor O_3 can reach levels exceeding that of the outdoors, and can even exceed the OSHA indoor limit of 100 ppb. However, even a small change in indoor O_3 levels can have a dramatic effect on people's total ozone exposure, given the large fraction of time people spend indoors (40). In most cases, deposition represents the dominant sink of ozone (Figure S7D). While product formation due to these surface losses (e.g., paint, textiles, skin) is not included in the model, volatile secondary organic products stemming from these reactions (12, 41) could represent an additional secondary effect of GUV_{222} on indoor air quality.

Figure 5C shows steady-state levels of OH as a function of ventilation and 222 nm light intensity. Sources of OH include O_3-alkene reactions (R3) and photochemistry (R4-5), while sinks are dominated by reactive losses (see also Figures S7F-G). In the absence of GUV_{222} irradiation, modeled OH is from alkene ozonolysis only, with predicted levels (~10^5 molec cm^{-3}) overlapping but falling on the low end of measured and modeled OH in unperturbed indoor spaces (which range from $6x10^4$-$1.6x10^6$ molec cm^{-3}) (42–50); this underestimate may arise from the omission of photolysis of trace species such as nitrous acid (HONO) or aldehydes, which may be important in some environments (51). As with O_3, GUV_{222} irradiation leads to increases in indoor levels of OH. At low to moderate light intensities, this increase in OH is mostly due to the alkene ozonolysis reaction, while at higher light intensities, ozone photolysis plays a larger role (Figure S7G). OH increases with increasing photochemistry (e.g., light intensity and ozone concentrations), but is substantially modulated by reactive losses with VOCs. VOC concentrations are higher at low ventilation rates (see Figure S7H), due to the buildup of emitted VOCs, which suppress OH concentrations. At high light intensities, steady-state OH levels can approach outdoor levels, matching or exceeding indoor OH measurements during transient events such as cleaning or cooking activities (13, 52). We do not examine the role of HONO, which can be present in high (ppb) levels indoors (50) and absorbs strongly at 222 nm (σ = 1.35 x 10^{-18} cm^2 (9)); HONO photolysis may lead to even higher OH levels than predicted here.

The production of O_3 and OH by GUV_{222}-driven chemistry and their subsequent reactions with VOCs leads to an increase in organic oxidation products (OVOCs and SOA). Steady-state levels and production rates of such products (assuming unit yields) are shown in Figures 5D and S7I. Concentrations increase with increased light intensity, and are especially high at low ventilation rates. Since more than one product molecule may be formed per oxidation reaction, and OVOCs may also be formed by surface reactions of O_3 or OH, these numbers likely represent lower limits. Of particular concern is the production of hazardous air pollutants (HAPs, such as CH_2O) and secondary organic aerosol, both of which may represent health hazards in the indoor environment. Concentrations of SOA are challenging to predict, as SOA production depends on the amounts and identity of the indoor VOCs, as well as on a host of reaction conditions. However, SOA levels on the order of a few $\mu g/m^3$ are reasonable (Figure S8); the production of SOA from 222 nm irradiation in realistic indoor settings is an important area of future research.

Conclusions

In this study, we have demonstrated that GUV_{222} light leads to the production of (1) ozone, (2) OH radicals, and (3) secondary organic species (OVOCs and SOA); these are in broad agreement with prior model predictions (23). The resulting concentrations of such secondary species can be substantially higher than are normally found in indoor environments; in extreme cases, these increases can be dramatic, leading to oxidation conditions more similar to those found in outdoor environments. The negative health impacts associated with the unavoidable generation of these secondary species – most importantly O_3, fine particular matter, and HAPs – thus need to be taken into account (and ideally mitigated) when considering the use of 222 nm disinfection in indoor spaces.

While a detailed analysis of the health impacts of GUV_{222} use (both the benefits from inactivation of airborne pathogens and the drawbacks from secondary pollutant formation) is beyond the scope of this work, our results offer some broad guidance as to the optimal use of GUV_{222} in indoor environments. Most importantly, GUV_{222} disinfection alone is not a safe substitute for ventilation as a means to control levels of indoor airborne pathogens, as it can lead to the buildup of indoor ozone and other pollutants to dangerous levels (Figure 5). However, GUV_{222} may be effectively used in conjunction with ventilation: relatively modest irradiation levels combined with carefully chosen ventilation conditions can greatly enhance the effective air change rate (Figure 5A), while limiting the levels of secondary pollutants (Figures 5B-D). Moreover, due to the unavoidable formation of secondary pollutants, GUV_{222} lights should be run at the lowest effective levels whenever possible. Further, the combination of GUV_{222} irradiation with air-cleaning technologies (e.g., sorbents for ozone and OVOCs, filters for particulate matter) may serve to minimize indoor secondary pollutant levels, potentially enabling safer use of GUV_{222} under poorly-ventilated environments. Quantifying the benefits and tradeoffs of these combined approaches (ventilation, GUV_{222} irradiation, and/or air cleaning) in terms of pathogen transmission, air pollutant levels, human health, and cost-effectiveness, is a critical next step toward ensuring healthier indoor environments.

Materials and Methods

a. Experimental Methods

Experiments are carried out in a 150 L Teflon chamber, outfitted with inlet ports (for introduction of clean air and trace species) and outlet ports (for sampling by analytical instrumentation). Clean air from a zero-air generator (Aadco Model 737) is sent into the chamber directly and through a water bubbler. Dilution rates are measured using acetonitrile, an inert dilution tracer (8.0×10^{-4} – 9.7×10^{-4} s^{-1}, 2.9 – 3.5 ACH). Most experiments are conducted at 22°C and ~25% RH; "higher RH" experiments are carried out at ~45% RH.

GUV_{222} light is provided by a single filtered KrCl excimer lamp (Ushio, Care222 B1 Illuminator, peak emission at 222 nm), centered directly above the Teflon chamber. Average irradiance within the chamber is ~45 $\mu W/cm^2$; light intensities are calculated from the lamp intensity profile provided by the manufacturer (53) (see Section S4.2). Most experiments are carried out at the full light intensity; for "low light" experiments, the lamp emission is attenuated by several layers of plastic, achieving a factor of ~5 reduction in intensity (determined by the reduction in the steady-state O_3 concentration). For the "O_3-only" experiments, the light is left off, and O_3 is introduced via a Pen-Ray ozone generator, with a steady-state O_3 concentration matching that of the GUV_{222} experiments (~100 ppb). Reaction conditions for each experiment are described in detail in Table S1.

For all VOC oxidation experiments, the chamber is first allowed to reach a steady-state concentration of O_3, either via 222 nm irradiation or direct addition. This is followed by the addition of 5.3 ppb of acetonitrile (the dilution tracer), 1.2 ppb of 1-butan-d9-ol (intended as an OH tracer, but not used here due to the relatively low OH levels), and 120 ± 11 $\mu g\ m^{-3}$ of

ammonium sulfate particles (to act as seed particles for any SOA production). Finally, the VOC (hexanal, cyclohexene, or (*R*)-(+)-limonene, 10 or 100 ppb) is added to chamber (see Section S3.1). Because the oxidants are already present in the chamber, oxidation begins immediately, so VOC injection is taken as t = 0.

Real-time measurements of gas- and particle-phase composition in the chamber are conducted using a suite of analytical instruments, summarized in Table S2. Ozone is measured by a UV absorption monitor (2BTech). Reactant VOC and OVOC products are monitored using a Vocus proton transfer-reaction mass spectrometer (PTR-MS, Tofwerk, Aerodyne Research, Inc. (54)), and an ammonium chemical ionization mass spectrometer (NH_4^+ CIMS, modified PTR3, see Zaytsev et al. (55)). Particle-phase products are quantified using a scanning mobility particle sizer (SMPS, TSI) and an aerosol mass spectrometer (Aerodyne Research, Inc. (56)). Data analysis and quantification approaches are described in Section S3.2.

b. Modeling Methods

The photooxidation chemistry in both the chamber (Figures 1-3) and in more realistic indoor environments (Figure 5) is described using a simple photochemical box model. The model uses rate constants and photochemical parameters from the literature (9–11, 24–26, 35, 57), and includes O_x and HO_x chemistry; the full set of reactions used is listed in Table S3. The only photolysis reactions included are of O_2 and O_3 (R1 and R3).

For simulations of chamber chemistry, the model includes a highly simplified oxidation scheme of the injected VOC. Model parameters (e.g. VOC starting concentration, light intensity, air-exchange rate, and RH) are matched to the experiment in question. O_3 deposition (which is likely small on Teflon surfaces) is not included.

For simulations of chemistry in a more realistic indoor environment (Figure 5), two "lumped" VOCs are included in the model: one (VOC1) that reacts with OH but not with O_3, and another (VOC2) that reacts with both OH and O_3. Rate constants for VOC1 are chosen based on typical values for indoor VOCs (Section S4.1 and Table S4); rate constants for VOC2 are assumed to be equal to those of limonene. OH yields from O_3 + VOC2 are assumed to by 0.86, equal to that of limonene (11). All oxidation reactions form lumped organic products that also can react with OH. VOC emission rates (84 ppb hr^{-1} and 4.2 ppb hr^{-1} for VOC1 and VOC2, respectively) are determined from previous measurements of OH and O_3 reactivities in indoor environments (33, 34); details of these calculations are given in Section S4.1.

3. Acknowledgements and Funding Sources

This work is supported by the U.S. National Science Foundation under grants ECS-2108811 and AGS-2129835 and the Harvard Global Institute. The authors thank Bella Nesti (Harvard University) for assisting with the initial phases of data analysis, and Jose Jimenez (University of Colorado Boulder) for helpful discussions.

4. References

1. W. F. Wells, M. W. Wells, T. S. Wilder, The environmental control of epidemic contagion: I. An epidemiologic study of radiant disinfection of air in day schools. *American Journal of Epidemiology* **35**, 97–121 (1942).

2. E. A. Nardell, Air Disinfection for Airborne Infection Control with a Focus on COVID-19: Why Germicidal UV is Essential†. *Photochemistry and Photobiology* **97**, 493–497 (2021).

3. Centers for Disease Control and Prevention, Upper Room Ultraviolet Germicidal Irradiation (UVGI) (2021) (May 17, 2023).

4. E. R. Blatchley, *et al.*, "Far UV-C Radiation: Current State-of Knowledge" (International Ultraviolet Association Task Force).

5. M. Buonanno, D. Welch, I. Shuryak, D. J. Brenner, Far-UVC light (222 nm) efficiently and safely inactivates airborne human coronaviruses. *Sci Rep* **10**, 10285 (2020).

6. D. B. Collins, D. K. Farmer, Unintended Consequences of Air Cleaning Chemistry. *Environ. Sci. Technol.* **55**, 12172–12179 (2021).

7. Q. Ye, *et al.*, Real-Time Laboratory Measurements of VOC Emissions, Removal Rates, and Byproduct Formation from Consumer-Grade Oxidation-Based Air Cleaners. *Environ. Sci. Technol. Lett.* **8**, 1020–1025 (2021).

8. M. C. Turner, *et al.*, Long-Term Ozone Exposure and Mortality in a Large Prospective Study. *Am J Respir Crit Care Med* **193**, 1134–1142 (2016).

9. J. Burkholder, *et al.*, "Chemical Kinetics and Photochemical Data for Use in Atmospheric Studies" (NASA Jet Propulsion Laboratory, 2020).

10. W. W. Nazaroff, C. J. Weschler, Indoor ozone: Concentrations and influencing factors. *Indoor Air* **32** (2022).

11. J. G. Calvert, *The Mechanisms of Atmospheric Oxidation of the Alkenes* (Oxford University Press, 2000).

12. A. Wisthaler, C. J. Weschler, Reactions of ozone with human skin lipids: Sources of carbonyls, dicarbonyls, and hydroxycarbonyls in indoor air. *Proceedings of the National Academy of Sciences* **107**, 6568–6575 (2010).

13. C. M. F. Rosales, *et al.*, Chemistry and human exposure implications of secondary organic aerosol production from indoor terpene ozonolysis. *Science Advances* **8**, eabj9156 (2022).

14. US EPA, Dose-Response Assessment for Assessing Health Risks Associated with Exposure to Hazardous Air Pollutants (2021) (May 2, 2023).

15. D. W. Dockery, *et al.*, An Association between Air Pollution and Mortality in Six U.S. Cities. *New England Journal of Medicine* **329**, 1753–1759 (1993).

16. R. Burnett, *et al.*, Global estimates of mortality associated with long-term exposure to outdoor fine particulate matter. *Proceedings of the National Academy of Sciences* **115**, 9592–9597 (2018).

17. H. O. T. Pye, C. K. Ward-Caviness, B. N. Murphy, K. W. Appel, K. M. Seltzer, Secondary organic aerosol association with cardiorespiratory disease mortality in the United States. *Nat Commun* **12**, 7215 (2021).

18. N. M. Donahue, G. T. Drozd, S. A. Epstein, A. A. Presto, J. H. Kroll, Adventures in ozoneland: down the rabbit-hole. *Phys. Chem. Chem. Phys.* **13**, 10848–10857 (2011).

19. H. Levy, Normal Atmosphere: Large Radical and Formaldehyde Concentrations Predicted. *Science* **173**, 141–143 (1971).

20. E. Bender, Disinfecting the air with far-ultraviolet light. *Nature* **610**, S46–S47 (2022).

21. Z. Peng, *et al.*, Significant Production of Ozone from Germicidal UV Lights at 222 nm. 2023.05.13.23289946 (2023).

22. M. F. Link, A. Shore, B. H. Hamdani, D. Poppendiek, Ozone Generation from a Germicidal Ultraviolet Lamp with Peak Emission at 222 nm (2023).

23. Z. Peng, S. L. Miller, J. L. Jimenez, Model Evaluation of Secondary Chemistry due to Disinfection of Indoor Air with Germicidal Ultraviolet Lamps. *Environ. Sci. Technol. Lett.* **10**, 6–13 (2023).

24. D. J. Stewart, *et al.*, The kinetics of the gas-phase reactions of selected monoterpenes and cyclo-alkenes with ozone and the NO3 radical. *Atmospheric Environment* **70**, 227–235 (2013).

25. S. M. Aschmann, J. Arey, R. Atkinson, Kinetics and Products of the Reactions of OH Radicals with Cyclohexene, 1-Methyl-1-cyclohexene, *cis* -Cyclooctene, and *cis* -Cyclodecene. *J. Phys. Chem. A* **116**, 9507–9515 (2012).

26. B. D'Anna, Ø. Andresen, Z. Gefen, C. J. Nielsen, Kinetic study of OH and NO 3 radical reactions with 14 aliphatic aldehydes. *Physical Chemistry Chemical Physics* **3**, 3057–3063 (2001).

27. A. Hansel, W. Scholz, B. Mentler, L. Fischer, T. Berndt, Detection of RO2 radicals and other products from cyclohexene ozonolysis with NH4+ and acetate chemical ionization mass spectrometry. *Atmospheric Environment* **186**, 248–255 (2018).

28. S. M. Aschmann, E. C. Tuazon, J. Arey, R. Atkinson, Products of the Gas-Phase Reaction of O3 with Cyclohexene. *J. Phys. Chem. A* **107**, 2247–2255 (2003).

29. S. Barua, S. Iyer, A. Kumar, P. Seal, M. Rissanen, An aldehyde as a rapid source of secondary aerosol precursors: Theoretical and experimental study of hexanal autoxidation. *EGUsphere*, 1–24 (2023).

30. B. C. Singer, *et al.*, Indoor secondary pollutants from cleaning product and air freshener use in the presence of ozone. *Atmospheric Environment* **40**, 6696–6710 (2006).

31. T. Wainman, J. Zhang, C. J. Weschler, P. J. Lioy, Ozone and limonene in indoor air: a source of submicron particle exposure. *Environmental Health Perspectives* **108**, 1139–1145 (2000).

32. B. Ma, *et al.*, Inactivation of Coronaviruses and Phage Phi6 from Irradiation across UVC Wavelengths. *Environ. Sci. Technol. Lett.* **8**, 425–430 (2021).

33. D. J. Price, *et al.*, Budgets of Organic Carbon Composition and Oxidation in Indoor Air. *Environ. Sci. Technol.* **53**, 13053–13063 (2019).

34. J. M. Mattila, *et al.*, Contrasting Chemical Complexity and the Reactive Organic Carbon Budget of Indoor and Outdoor Air. *Environ. Sci. Technol.* **56**, 109–118 (2022).

35. T. Grøntoft, M. R. Raychaudhuri, Compilation of tables of surface deposition velocities for O3, NO2 and SO2 to a range of indoor surfaces. *Atmospheric Environment* **38**, 533–544 (2004).

36. International Commission on Non-Ionizing Radiation Protection (ICNIRP), Guidelines on limits of exposure to ultraviolet radiation of wavelengths between 180 nm and 400 nm (incoherent optical radiation). *Health Phys* **87**, 171–186 (2004).

37. American Conference of Governmental Industrial Hygienists, *2023 Threshold Limit Values (TLVs) and Biological Exposure Indices (BEIs)* (2023) (May 3, 2023).

38. E. Eadie, *et al.*, Far-UVC (222 nm) efficiently inactivates an airborne pathogen in a room-sized chamber. *Sci Rep* **12**, 4373 (2022).

39. , ASHRAE/ANSI Standard 62.1-2022. Ventilation and Acceptable Indoor Air Quality (2022).

40. C. J. Weschler, Ozone's Impact on Public Health: Contributions from Indoor Exposures to Ozone and Products of Ozone-Initiated Chemistry. *Environ Health Perspect* **114**, 1489–1496 (2006).

41. H. Wang, G. Morrison, Ozone-surface reactions in five homes: surface reaction probabilities, aldehyde yields, and trends. *Indoor Air* **20**, 224–234 (2010).

42. C. J. Weschler, H. C. Shields, Production of the Hydroxyl Radical in Indoor Air. *Environ. Sci. Technol.* **30**, 3250–3258 (1996).

43. C. J. Weschler, H. C. Shields, Measurements of the Hydroxyl Radical in a Manipulated but Realistic Indoor Environment. *Environ. Sci. Technol.* **31**, 3719–3722 (1997).

44. N. Carslaw, A new detailed chemical model for indoor air pollution. *Atmospheric Environment* **41**, 1164–1179 (2007).

45. M. S. Waring, J. R. Wells, Volatile organic compound conversion by ozone, hydroxyl radicals, and nitrate radicals in residential indoor air: Magnitudes and impacts of oxidant sources. *Atmospheric Environment* **106**, 382–391 (2015).

46. N. Carslaw, L. Fletcher, D. Heard, T. Ingham, H. Walker, Significant OH production under surface cleaning and air cleaning conditions: Impact on indoor air quality. *Indoor Air* **27**, 1091–1100 (2017).

47. S. Gligorovski, C. J. Weschler, The Oxidative Capacity of Indoor Atmospheres. *Environ. Sci. Technol.* **47**, 13905–13906 (2013).

48. E.-A. Fiorentino, *et al.*, Measurements and Modelling of OH and Peroxy Radicals in an Indoor Environment Under Different Light Conditions and VOC Levels. *Atmospheric Environment* **292**, 119398 (2023).

49. M. Mendez, *et al.*, Identification of the major HOx radical pathways in an indoor air environment. *Indoor Air* **27**, 434–442 (2017).

50. E. Gómez Alvarez, *et al.*, Unexpectedly high indoor hydroxyl radical concentrations associated with nitrous acid. *Proceedings of the National Academy of Sciences* **110**, 13294–13299 (2013).

51. S. F. Kowal, S. R. Allen, T. F. Kahan, Wavelength-Resolved Photon Fluxes of Indoor Light Sources: Implications for HOx Production. *Environ. Sci. Technol.* **51**, 10423–10430 (2017).

52. E. Reidy, *et al.*, Measurements of Hydroxyl Radical Concentrations during Indoor Cooking Events: Evidence of an Unmeasured Photolytic Source of Radicals. *Environ. Sci. Technol.* **57**, 896–908 (2023).

53. Ushio, Inc., Care222 Technical Specification Sheet (May 3, 2023).

54. J. Krechmer, *et al.*, Evaluation of a New Reagent-Ion Source and Focusing Ion–Molecule Reactor for Use in Proton-Transfer-Reaction Mass Spectrometry. *Anal. Chem.* **90**, 12011–12018 (2018).

55. A. Zaytsev, *et al.*, Using collision-induced dissociation to constrain sensitivity of ammonia chemical ionization mass spectrometry (NH4+ CIMS) to oxygenated volatile organic compounds. *Atmos. Meas. Tech.* **12**, 1861–1870 (2019).

56. P. F. DeCarlo, *et al.*, Field-Deployable, High-Resolution, Time-of-Flight Aerosol Mass Spectrometer. *Anal. Chem.* **78**, 8281–8289 (2006).

57. S. M. Saunders, M. E. Jenkin, R. G. Derwent, M. J. Pilling, Protocol for the development of the Master Chemical Mechanism, MCM v3 (Part A): tropospheric degradation of non-aromatic volatile organic compounds. *Atmospheric Chemistry and Physics* **3**, 161–180 (2003).